SolarPACES 2024, 30th International Conference on Concentrating Solar Power, Thermal, and Chemical Energy Systems

Analysis and Simulation of CSP and Hybridized Systems

https://doi.org/10.52825/solarpaces.v3i.2432

© Authors. This work is licensed under a Creative Commons Attribution 4.0 International License

Published: 28 Nov. 2025

# Investigation on the Injection of Exhaust Air Into Cavity Receivers

Koda Boldt<sup>1</sup>, Aidan McConnehey<sup>1</sup>, and Todd Otanicar<sup>1,\*</sup>

<sup>1</sup>Boise State University, USA

\*Correspondence: Todd Otanicar, toddotanicar@boisestate.edu

Abstract. Concentrating solar thermal (CST) systems stands out as a promising renewable energy technology, leveraging radiative heat transfer to convert solar irradiance into thermal energy. Central receiver systems (CRS), a form of CST, demonstrate potential for diverse industrial applications due to their ability to operate at high temperatures. However, optimizing their efficiency remains a challenge, particularly regarding the utilization of air as a heat transfer fluid (HTF). This study investigates the impact of exhaust air reinjection on the performance of cavity receiver systems in CST. Previous research has explored similar concepts, but gaps remain in directly modeling exhaust air return, especially in the context of cavity receivers. Using a finite element method (FEM) model this research examines various parameters affecting exhaust air injection, including injection ring height and outlet air flow velocity. Results indicate a dependency between exhaust air reinjection velocity, total mass flow rate, and the air return ratio (ARR). Higher injection velocities, coupled with increased mass flow rates, lead to greater exhaust air loss and lower ARR values. Through parametric analysis, insights are gained into the geometry parameters crucial for optimizing ARR and enhancing receiver efficiency. The highest ARR of greater than 95% is achievable when the air is injected close to the aperture in the radial directions and the fluid velocity is minimized through lower flowrates or increased inlet boundary area. These findings contribute to advancing the understanding and design of cavity receiver systems for improved renewable energy utilization.

Keywords: Cavity Receiver, Fluid Flow, Porous Media

### 1. Introduction

Applications such as power generation [1], and many industrial processes [2], operate at extremely high temperatures which are required for increases in efficiency in power generation and necessary for some processes. As such, during the process of using thermal energy that is generated through the use of a porous cavity system applied to concentrated solar thermal (CST) systems , the working fluid exits the process at a low temperature compared to the supplied temperature. This lower temperature, however, is still high with respect to the ambient air. The porous cavity receivers (CR) that have been the focus of the present research are defined to be open, as such the air is directly absorbed through the aperture. As such, injecting the process outlet air back into the inlet of the porous CR has been common practice.

This interaction between the outlet process air and the inlet receiver air temperatures has been handled in three ways. The first assumes that the inlet receiver temperature is some higher-than-ambient value that represents the addition of return air from the process. The second method assumes the proportion of the return air that is reabsorbed by the receiver and calculates the effective inlet temperature based on this proportion of return air being absorbed,

the return air temperature, and the ambient air temperature by the use of a thermodynamic mixing equation. The third and final method involves setting up a complex finite element method (FEM) model to include the geometry of the ambient air domain and model the reinjection directly.

Each method has its own limitations and assumptions. The first method of assuming a higher inlet temperature accounts for the higher inlet temperature in overall receiver performance. However, its resolution does not lend itself to understanding how varying return air temperatures and ambient temperatures affect the effective inlet air temperature. For this reason, the method of assuming an inlet air temperature will not be further investigated by present research. The second method is able to account for variate return air and ambient air temperatures; however, it relies heavily on the assumed proportion of return air. The third method is much more accurate as it is able to not only resolve the effects of variate return air and ambient air temperatures but is also able to model the mixing of the two air streams directly.

Three papers which were reviewed studied the reinjection of return air: M.J. Marcos et al. [3], H. Stadler et al. [4], and M. Cagnoli et al. [5]. M.J. Marcos et al. analyze a return air system in which the return air was flown outside-in through the absorbing porous media, acting as a counter-flow heat exchanger. Their findings conclude that the fraction of air returned to the system, the air return ratio (ARR), is variable depending on the operational conditions. The two other studies done by H. Stadler et al. and M. Cagnoli et al. are performed on open volumetric cup receivers. These studies have concluded that the parameters involving the reinjection, such as total mass flow rate and return air reinjection velocity, are largely responsible for variable ARRs. These studies do not take into account the added complexity of modeling the return air directly and whether that computational cost is advantageous to the design of porous cavity receivers.

The method of modeling the reinjection directly comes at the cost of computational efficiency and model simplicity but provides the best insight into receiver performance. The question this research will seek to answer is whether this added complexity and computational cost is a necessity, or if an approximate ARR can be assumed for a variety of return air injection configurations. The study will answer this research question through the use of FEM models developed to analyze open spherical-cavity receivers.

# 2. Methodology

To comprehensively evaluate the effects of return air reinjection on cavity receivers in CST systems, a detailed FEM model was developed [6]. This model captures both fluid flow and heat transfer dynamics using a combination of the Brinkman formulation for fluid flow in porous media, alongside the Local Thermal Non-Equilibrium (LTNE) method for energy balance. A.L. Avila-Marin et al. elaborate on this methodology for their work on the comparison of radiative modeling methodologies for porous solar receivers [7]. By incorporating these advanced techniques, the study ensures an accurate representation of the complex interactions between ambient and return air flows, and their influence on overall receiver performance. This section outlines the governing equations, boundary conditions, and key assumptions used to model the system, while also discussing the methods applied to assess the ARR under varying operational conditions.

The fluid flow is governed by two equations. The first governing equation is the conservation of mass. As this research will treat the working fluid, air, as an incompressible gas, the density is able to be treated as a constant and multiplied directly to the differential terms. Equation 1 describes the conservation of mass as used in the present research.

$$\rho_f \nabla \cdot \boldsymbol{U} = 0 \tag{1}$$

The second equation that governs the fluid flow is the conservation of momentum. This equation includes two terms to account for the porous media: the Brinkman term, and the Forchheimer term. The Brinkman term is the second term on the right-hand side of Equation 2, it is responsible for accounting for the shear stress to which the fluid is subjected because of the solid portion of the porous media. The Forchheimer term is the far-right term in Equation 2 and has been added to the standard formulation of the Brinkman equation in order to account for drag forces. This method has also been used by S. Sharma, and P. Talukdar to analyze volumetric absorbing receivers [8].

$$\frac{\rho_f}{\phi} \nabla \cdot \left( \frac{\mathbf{U} \cdot \mathbf{U}}{\phi} \right) = -\nabla P + \nabla \cdot \left[ \frac{\mu_f}{\phi} \left( \nabla \mathbf{U} + (\nabla \mathbf{U})^T - \frac{2}{3} \nabla \cdot \mathbf{U} I \right) \right] - \mathbf{F}$$
 (2)

The Forchheimer term can be calculated as shown in Equation 3. Here  $\mathcal{C}_F$  is the inertial constant, and K is the permeability of the fluid. Equations 4 and 5 define the permeability and inertial constant, respectively. These formulations are consistent with those used by Z. Wu, et al. [9]. These terms are highly dependent on the pore diameter,  $d_p$ , and the porosity,  $\phi$ , of the porous media.

$$\mathbf{F} = \left(-\frac{\mu_f}{K} + \frac{C_F}{\sqrt{K}}\rho_f |\mathbf{U}|\right) \mathbf{U} \tag{3}$$

$$K = \frac{d_p^2}{1,039 - 1,002\phi} \tag{4}$$

$$C_F = \frac{0.5138\phi^{-5.739}}{d_p} \tag{5}$$

In this study, the flow was modeled under the incompressible assumption. The study focuses on the mixing behavior of the injection ring air (250 °C) and ambient room temperature air within the receiver aperture. While the thermal environment leads to substantial temperature differences, the Mach numbers in the aperture region remain well below 0.3, and pressure variations are small relative to the absolute pressure. As a result, density changes due to compressibility are negligible compared to those arising from thermal effects. This approach is appropriate for the aperture region, where the primary concern is the relative contribution of the two inlet streams rather than detailed compressible dynamics.

This research will rely on the LTNE as its method of solving the conjugate heat transfer between the porous media and the fluid which flows through it. This method allows for accurate approximate solutions to be calculated as it models the fluid and the solid separately. As the two volumes will be treated separately, two heat transfer equations are required: one for the fluid phase, and one for the solid phase. Equation 6 and 7 handle the energy balance for the fluid and solid phases, respectively.

$$\nabla \cdot \left(\rho_f C_{P,f} \mathbf{U} T_f\right) = \nabla \cdot \left(k_{fe} \nabla T_f\right) + h_v \left(T_s - T_f\right) \tag{6}$$

$$\nabla \cdot (k_{se} \nabla T_s) + h_v (T_f - T_s) = S_r \tag{7}$$

The energy balance equations are based on the temperature differences present between the solid,  $T_s$ , and fluid,  $T_f$ . The equations are also reliant on the thermal conductivity of each phase. As the media is porous and both phases are present in the same domain, effective thermal

conductivities must be calculated. Equations 8 and 9 are responsible for calculating the effective thermal conductivities of the porous media. Finally, a volumetric convective heat transfer correlation is described in Equation 10. This formulation was developed by Z. Wu et al. [10]. The formulation is dependent on the Reynolds number. Equation 11 defines the Reynolds number with respect to the pore diameter of the porous media. The solid phase energy balance also includes a radiative heat source term,  $S_r$ , that is responsible for the heat input due to the solar irradiance. This term will be defined in the context of the RTE.

$$k_{fe} = \phi k_f \tag{8}$$

$$k_{se} = 3(1 - \phi)k_s \tag{9}$$

$$h_v = \frac{k_f Re^{0.438}}{d_p^2} (37.504\phi^{0.38} - 109.94\phi^{1.38} + 166.65\phi^{2.38} - 86.98\phi^{3.38})$$
 (10)

$$Re = \frac{\rho_f |\mathbf{U}| d_p}{\mu_f} \tag{11}$$

The radiative heat source term present in Equation 7 is crucial to the model. Without it, no heat transfer would be possible. This term accounts for the radiative heat transfer through the receiver due to the solar irradiance applied to its inner surface. The radiative heat source term separates the diffuse radiative component,  $G_d$ , from the collimated radiative component,  $G_c$ . Equation 12 defines the radiative heat source term.

$$S_r = \kappa_a (4\sigma T_S^4 - G_d) + \kappa_S G_c \tag{12}$$

In order to calculate the diffuse radiation, the RTE must be solved. For this research the P1 approximation will be used to compute the radiative heat transfer. This method is detailed in M.F. Modest's *Radiative Heat Transfer* [11]. It is a computationally efficient method that performs the necessary calculations by accurately separating the collimated radiation from the diffuse. The RTE Equation, 13, is dependent on knowing the collimated component. The collimated component is defined as the energy from solar irradiance absorbed by the solid phases throughout its thickness and can be referenced using Equation 14. This is calculated by employing the use of the extinction coefficient,  $\beta$ . Two other porous media characteristics must also be described: the absorbing coefficient,  $\kappa_a$ , and the scattering coefficient,  $\kappa_s$ . The extinction, absorbing, and scattering coefficients are all functions of the solid phase's emissivity,  $\epsilon$ , the pore diameter, and the porosity. The three coefficients are defined by Equations 15, 16, and 17, respectively.

$$-\nabla \cdot \left(\frac{1}{3(\kappa_a + \kappa_s)}\nabla G_d\right) = \kappa_a (4\sigma T_s^4 - G_d) + \kappa_s G_c \tag{13}$$

$$G_c = q_0 e^{-\beta t(r)} \tag{14}$$

$$\kappa_a = \frac{3\varepsilon(1-\phi)}{2d_p} \tag{15}$$

$$\kappa_{s} = \frac{3(2-\varepsilon)(1-\phi)}{2d_{p}} \tag{16}$$

$$\beta = \kappa_a + \kappa_s = \frac{3(1 - \phi)}{d_p} \tag{17}$$

An important boundary condition when computing radiative heat transfer in porous media is the wall condition. Equation 18 is implemented at surfaces where the porous media meets a solid wall. This equation will account for the heat dissipation through the wall. The wall is treated as a perfect absorber, that is,  $\varepsilon_w = 1$ .

$$S_w = -\varepsilon_w \sigma (T_s^4 - T_a^4) \tag{18}$$

A set of inlet airflow boundary conditions were developed in order to model the exhaust air reinjection directly. Rather than assuming an ARR, this model directly simulates the reinjection of return air by adding an inlet air stream for the return air. This boundary condition sets the mass flow rate of the inlet air stream. Here the mass flow rate,  $\dot{m}$ , is set to be equal to the mass flow rate at the outlet boundary. This is done as it is assumed that the receiver will be operating at a state of equilibrium. For this case, it is possible to calculate the actual ARR based on the average temperature at the receiver inlet, the return air temperature, and the ambient temperature. The equations calculating the ARR, and average inlet temperature are given by Equations 19 and 20, respectively.

$$ARR = \frac{T_{i,avg} - T_a}{T_r - T_a} \tag{19}$$

$$T_{i,avg} = \frac{1}{A_i} \oint T_i dS_i \tag{20}$$

The boundary conditions for the direct modeling of return air reinjection are defined in Figure 1. The inlet air domain, b, includes a region of ambient air and extends through the aperture and up to the surface of the porous media. The inlet air domain includes an open boundary condition, a, the return air inlet, h, and finally regions of slipping walls, g. The porous media region, d, exhibits both the physics of the solid and fluid using the LTNE method which is applied to its domain. This domain is divided into 32 regions, each with its own porosity. Finally, the outlet air domain, e, extends from the outer surface of the porous media to the exit boundary condition, f. This outlet air domain includes no-slip wall conditions on all external boundaries, i.

a Open boundary
b Inlet air domain
c Aperture
d Porous media domain
e Outlet air domain
f Outlet boundary
g Slipping wall boundary
h Return air inlet boundary
i No-slip wall boundary

Figure 1. Spherical cavity receiver, domains and boundaries

## 3. Results

Using the finite element analysis (FEA) model, a series of simulations were conducted to examine the effects of varying three key parameters: mass flow rate, injection ring height (height of the boundary h, as shown in Figure 1), and the reinjection ring radius (the radial location of the boundary h, as shown in Figure 1) on the ARR of the cavity receiver. The objective was to better understand how these parameters influence the reinjection of exhaust air into the system and to derive insights that can optimize the performance of cavity receivers in CST applications.

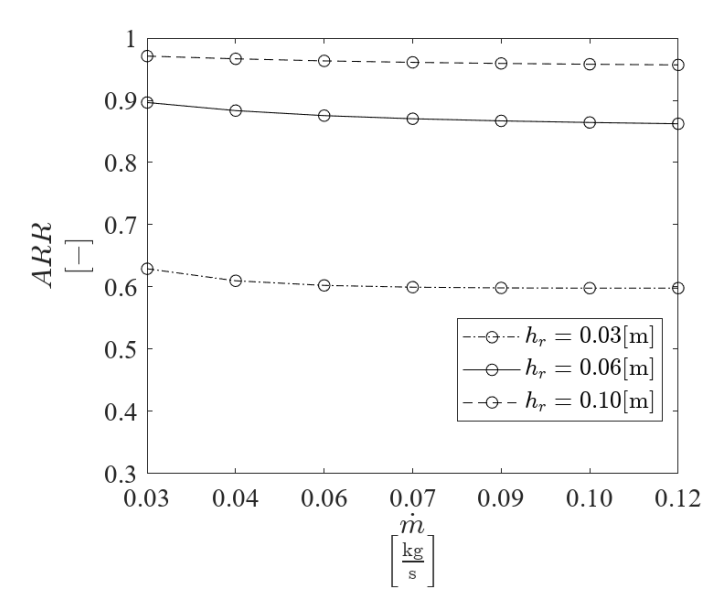


Figure 2. Air return ratio vs. mass flow rate, for variable injection ring height

The first set of results (Figure 2) illustrates the relationship between mass flow rate and ARR for three reinjection ring heights: 0.03 m, 0.06 m, and 0.10 m. As the injection ring height increases, the ARR also increases, indicating a more effective air return at greater heights. Conversely, increasing the mass flow rate reduces the ARR due to higher fluid velocities leading to exhaust air loss. However, this dependency on mass flow rate diminishes with an increase in ring height, as evidenced by the flatter slope for the tallest ring compared to the shortest one.

Next, a comparison of the reinjection system with varying porosities is presented in Table 1. The results show that the ARR values remain nearly identical between the simulations with a receiver porosity of 50% and 90%, indicating that the porosity of the receiver, and therefore the pressure drop across it, does not significantly affect the quality of air returned to the system.

| 1 1 41 37 1 14        |                      | 1 1               | 1 1            | 4: 0 1         |
|-----------------------|----------------------|-------------------|----------------|----------------|
| ,                     |                      |                   | •              |                |
| rable 1. Companson of | ali relum ralios ior | variable receiver | porosities and | mass now rates |

| Injection Velocity | Mass Flow Rate | Air Return Ratio<br>ε = 0.90 | Air Return Ratio<br>ε = 0.50 |
|--------------------|----------------|------------------------------|------------------------------|
| [m/s]              | [kg/s]         | [-]                          | [-]                          |
| 0.200              | 0.030          | 0.593                        | 0.598                        |
| 0.300              | 0.045          | 0.578                        | 0.582                        |
| 0.400              | 0.060          | 0.572                        | 0.576                        |
| 0.500              | 0.075          | 0.570                        | 0.573                        |
| 0.600              | 0.090          | 0.568                        | 0.572                        |
| 0.700              | 0.104          | 0.567                        | 0.571                        |
| 0.800              | 0.119          | 0.567                        | 0.570                        |

Figure 3 presents results from a trial similar to Figure 1, but this time varying the reinjection ring radius (with intervals of 0.32 m, 0.43 m, and 0.57 m) at a fixed ring height of 0.05 m. As expected, increasing the mass flow rate leads to a reduction in ARR, though larger radii exhibit higher ARRs (approximately 85% for the largest radius) compared to the smallest radius, which shows an ARR of around 60%.

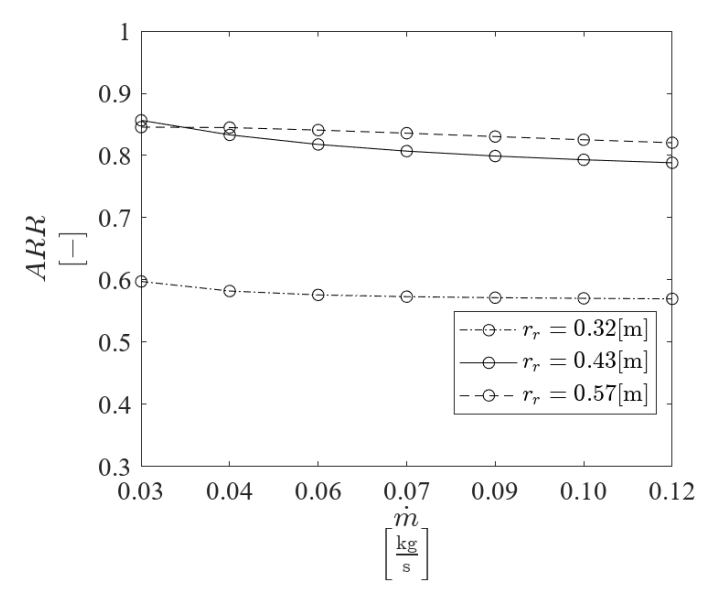


**Figure 3.** Air return ratio vs. mass flow rate, for variable injection ring radii ( $h_r = 0.05 \text{ m}$ )

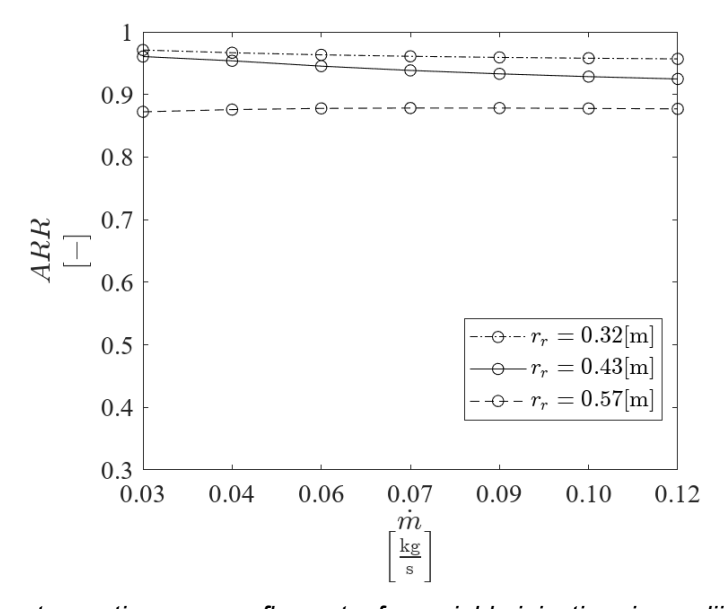


**Figure 4.** Air return ratio vs. mass flow rate, for variable injection ring radii ( $h_r = 0.10 \text{ m}$ )

In Figure 4, the same analysis was conducted but with a reinjection ring height of 0.10 m. This configuration resulted in the highest ARR values across the tests, with the narrowest radius achieving an ARR of over 95% and the largest radius having an ARR in the high 80% range. Interestingly, these results are inverted when compared to the shorter reinjection ring height of 0.05 m. This is most likely due to the taller reinjection ring contributing lower velocities, which are more easily captured by the receiver when they are more localized to the aperture. The effects of mass flow rate varied for different radii: the smallest radius (0.32 m) maintained a nearly constant ARR, the middle radius (0.43 m) showed a typical decrease in ARR as mass flow rate increased, and the largest radius (0.57 m) demonstrated an increase in ARR with higher mass flow rates.

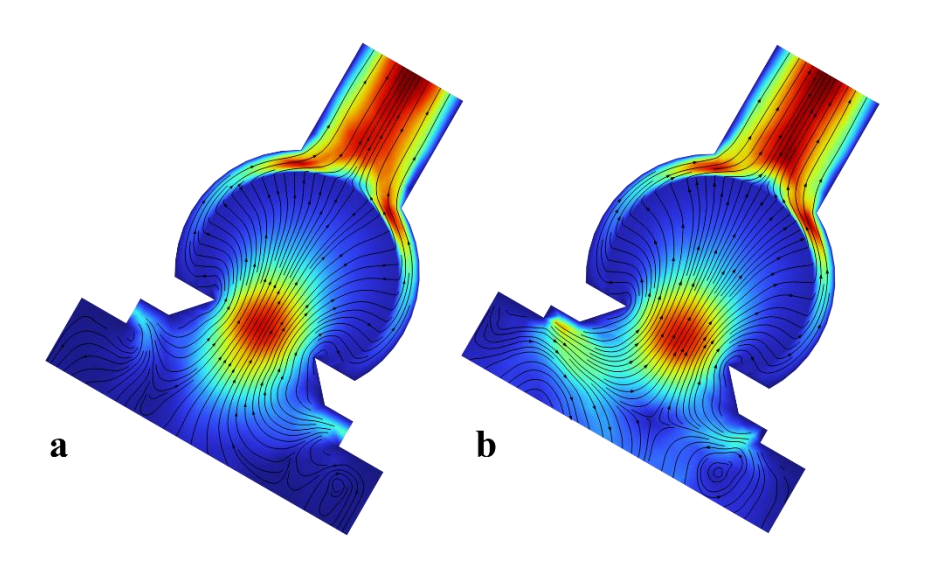


**Figure 5.** Velocity streamlines; a) tall injection ring ( $h_r = 0.10 \text{ m}$ ), b) short injection ring ( $h_r = 0.05 \text{ m}$ )

In Figure 5, velocity streamlines overlayed on a slice taken from the middle of the cavity are shown for two different injection ring heights: 0.10 m (left, plot (a)) and 0.05 m (right, plot (b)). The reinjection radius for both plots was 0.43 m, and the mass flow rate was set at 0.075 kg/s. The taller ring exhibited more streamlines exiting the open boundary compared to the shorter ring, which suggests greater air leakage in the former. Maximum fluid velocities were 0.979 m/s for the tall ring and 0.990 m/s for the short ring, showing negligible differences in velocity but notable differences in flow patterns.

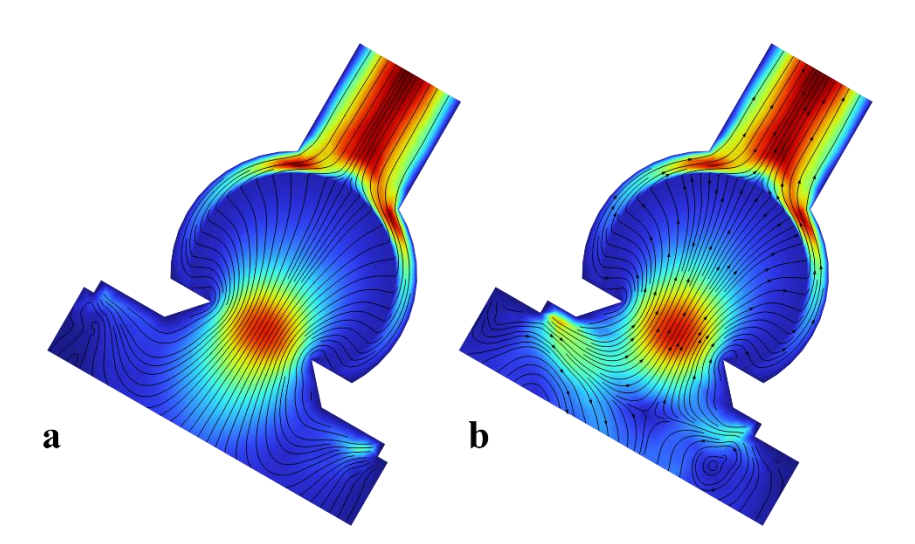


**Figure 6.** Velocity streamlines; a) wide injection ring  $(r_r = 0.57 \text{ m})$ , b) narrow injection ring  $(r_r = 0.43 \text{ m})$ 

Figure 6 explores the effects of reinjection ring radius on the flow patterns, with the left plot (a) showing results for a wide reinjection radius (0.57 m) and the right plot (b) for a narrow radius (0.43 m). The wider ring displayed a smoother and more consistent flow pattern, though more streamlines exited the receiver compared to the narrow ring, which had slight non-uniformities in the flow. The maximum velocities were 0.987 m/s for the wide ring and 0.990 m/s for the narrow ring.

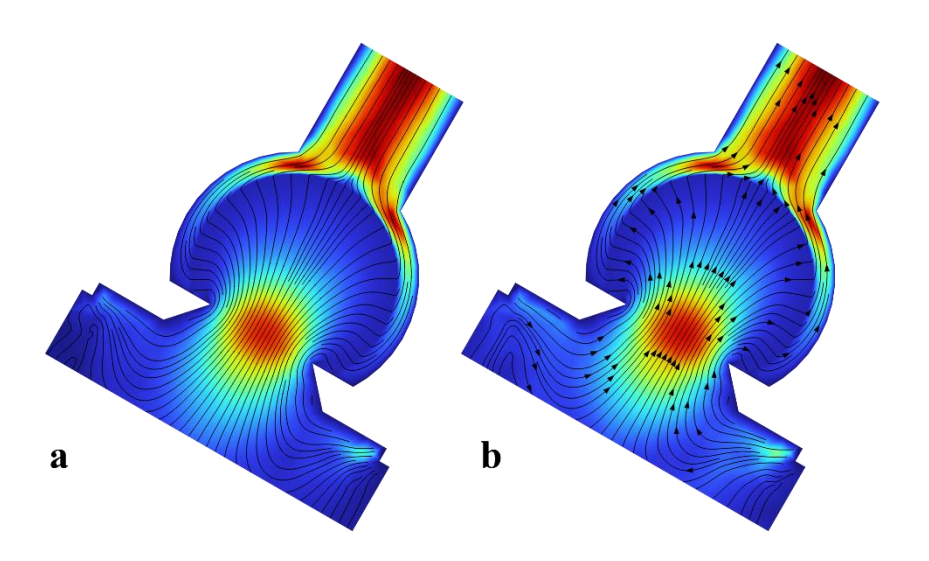


Figure 7. Velocity streamlines; a) slow return flow (m = 0.03 [kg/s]), b) fast return flow (m = 0.12 [kg/s])

Finally, Figure 7 highlights the effects of varying mass flow rates, with plot (a) showing a flow rate of 0.03 kg/s and plot (b) showing 0.12 kg/s. Both plots use a wide radius (0.57 m) and a short height (0.05 m). The streamlines in both configurations were similar, except that the higher mass flow rate led to significantly larger fluid velocities (the maximums being 1.56 m/s vs. 0.399 m/s), as indicated by the larger arrows on the streamlines.

### 4. Conclusions

The results of this study provide valuable insights into the behavior of cavity receiver systems with exhaust air reinjection. The findings reveal that the reinjection ring height and radius significantly affect the air return ratio (ARR), with larger reinjection ring heights and radii generally leading to higher ARRs. However, mass flow rate plays a complex role: while increasing mass flow generally reduces ARR due to higher fluid velocities, this effect is less pronounced for larger reinjection rings. Additionally, the receiver porosity does not significantly impact the air return behavior, simplifying considerations for receiver design.

Through detailed parametric analysis, it is clear that optimizing the geometry and operational conditions of the reinjection system is crucial for maximizing the ARR of cavity receivers in concentrated solar power applications. These findings contribute to the ongoing development of high-efficiency renewable energy systems, providing a deeper understanding of the flow dynamics and air return mechanisms in cavity receivers. Future work could focus on further refining the FEA models and expanding the scope to include more complex reinjection configurations and real-world operational conditions.

# Data availability statement

For reasons of maintaining intellectual property, the information and data presented in this paper is limited.

## **Author contributions**

**Koda Boldt:** Conceptualization, Methodology, Analysis, Data Curation, Writing – Original Draft, Writing – Review & Editing. **Aidan McConnehey:** Conceptualization. **Todd Otanicar:** Conceptualization, Supervision, Funding Acquisition, Writing – Review & Editing.

# **Competing interests**

The authors declare that they have no competing interests.

# **Funding**

This work was partially funded by the U.S. Department of Energy Solar Energy Technologies Office under award number DE-EE0009806.

## References

- [1] O. Behar, A. Khellaf, K. Mohammedi, "A review of studies on central receiver solar thermal power plants," Renewable Sustainable Energy Reviews, vol. 23, pp. 12-39, 2013.
- [2] T. Melchior, C. Perkins, A.W. Weimer, A. Steinfeld, "A cavity-receiver containing a tubular absorber for high-temperature thermochemical processing using concentrated solar energy," International Journal of Thermal Sciences, vol. 47, pp. 1,496-1,503, 2008.
- [3] M.J. Marcos, M. Romero, and S. Palero, "Analysis of air return alternatives for CRS-type open volumetric receiver," Energy, vol. 29, pp. 677-686, 2004.
- [4] H. Stadler, A. Tiddens, P. Schwarzbozl, F. Gohring, T. Baumann, and J. Trautner, "Improved performance of open volumetric receivers by employing an external air return system," Solar Energy, vol. 155, pp. 1,157-1,164, 2017.
- [5] M. Cagnoli, A. Froio, L. Savoldi, and R. Zanino, "Multi-scale modular analysis of open volumetric receivers for central tower CSP systems," Solar Energy, vol. 190, pp. 195-211, 2019.
- [6] COMSOL, "COMSOL Multiphysics," 2024. [Online]. Available: https://www.comsol.com/.
- [7] A.L. Avila-Marin, J. Fernandez-Reche, and A. Martinez-Tarifa, "Modelling strategies for porous structures as solar receivers in central receiver systems: A review," Renewable and Sustainable Energy Reviews, vol. 111, pp. 15-33, 2019.
- [8] S. Sharma, and P. Talukdar, "Thermo-mechanical analysis of a porous volumetric solar receiver subjected to concentrated solar radiation," Solar Energy, vol. 247, pp. 41-54, 2022.
- [9] Z. Wu, C. Caliot, F. Bai, G. Flamant, Z. Wang, J. Zhang, and C. Tian, "Experimental and numerical studies of the pressure drop in ceramic foams for volumetric solar receiver applications," Applied Energy, vol. 87, pp. 504-513, 2010.
- [10] Z. Wu, C. Caliot, G. Flamant, and Z. Wang, "Numerical simulation of convective heat transfer between air flow and ceramic foams to optimize volumetric solar air receiver performances," International Journal of Heat and Mass Transfer, vol. 54, pp. 1,527-1,537, 2011.
- [11] M.F. Modest, "Radiative Heat Transfer," Academic Press, 2003.